Prediction of Two-Dimensional High-T_C *f*-electron Ferromagnetic Semiconductor

Bing Wang,[†,§] Xiwen Zhang,[‡] Yehui Zhang,[†] Shijun Yuan,[†] Yilv Guo,[†] Shuai Dong,[*,†] and Jinlan Wang [*,†]

[†] School of Physics, Southeast University, Nanjing 211189, China

[§] Institute for Computational Materials Science, School of Physics and Electronics, Henan University, Kaifeng 475004, China

[‡] School of Mechanism Engineering & School of Physics, Southeast University, Nanjing 211189, China

*Corresponding Author E-mail: jlwang@seu.edu.cn; sdong@seu.edu.cn

1. The structure and ELF of GdI_2 bulk.

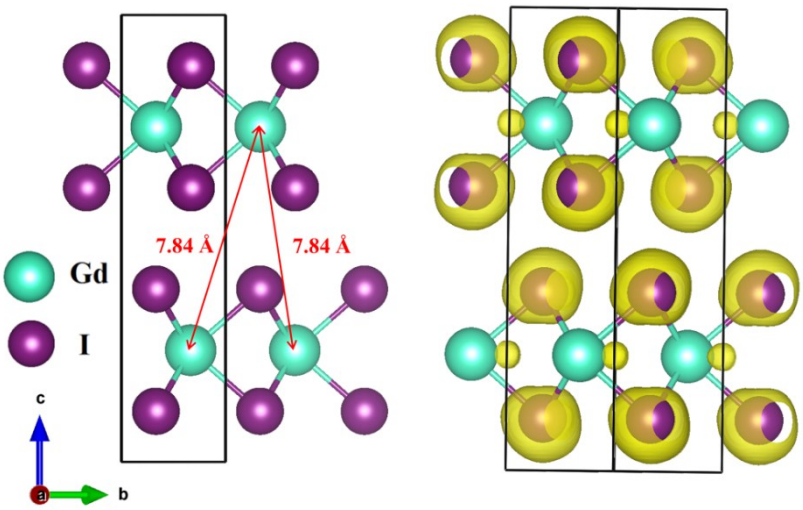

Figure S1. Structure (a) and electron localization function (b) of bulk GdI_2.

2. Mechanical stability of GdI_2 monolayer.

To verify the mechanical stability of GdI_2 monolayer, its elastic constants were calculated to be $C_{11} = C_{22} = 36.4$ N/m, $C_{12} = 10.9$ N/m, and $C_{66} = 12.8$ N/m. It can be seen that these values satisfy Born criteria[1] for 2D hexagonal crystal, namely, C_{11}, C_{22}, $C_{44} > 0$ and $C_{11}C_{22}\text{-}C_{12}^2 > 0$, confirming the GdI_2 monolayer is mechanically stable. The in-plane Young's modulus (Y), which can be deduced from the elastic constants by $Y = (C_{11}^2 - C_{12}^2)/C_{11}$, was computed to be 33.2 N/m. The value is comparable to germanene (42 N/m),[2] suggesting that GdI_2 monolayer has good mechanical properties.

3. Spin density of FM and AFM states.

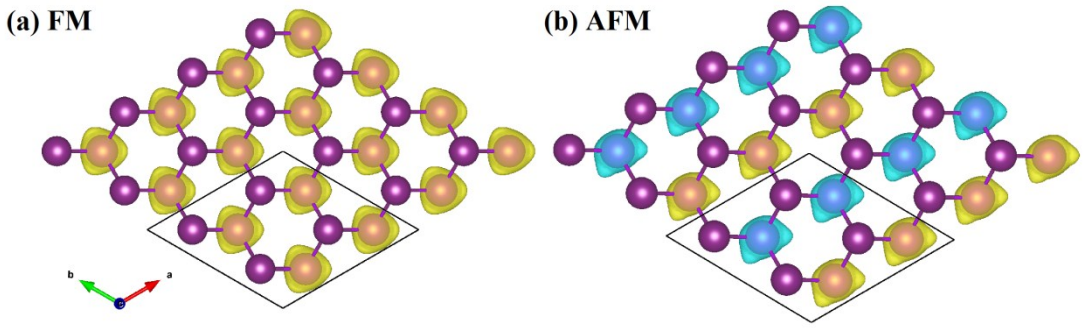

Figure S2. Spin density of FM (a) and AFM (b) states of GdI_2 monolayer.

4. Band structure of GdI_2 monolayer with spin-orbit coupling (SOC).

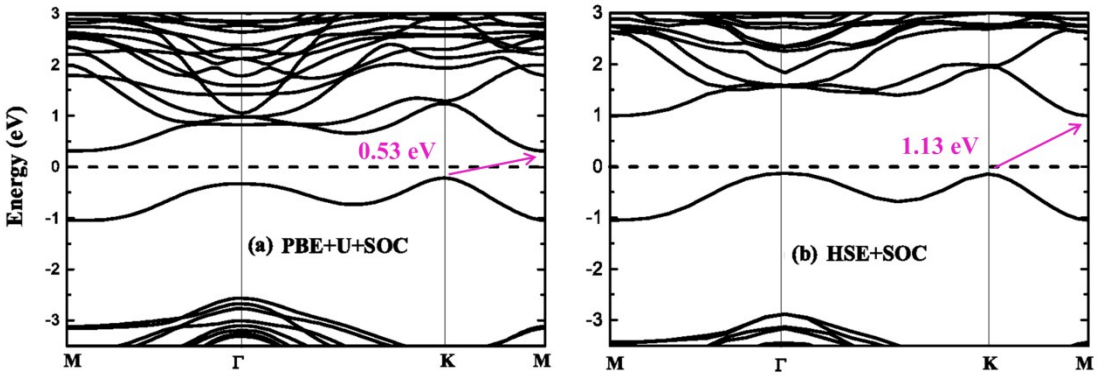

Figure S3. Band structure of GdI_2 monolayer with SOC.

5. Density of states of GdI_2 monolayer.

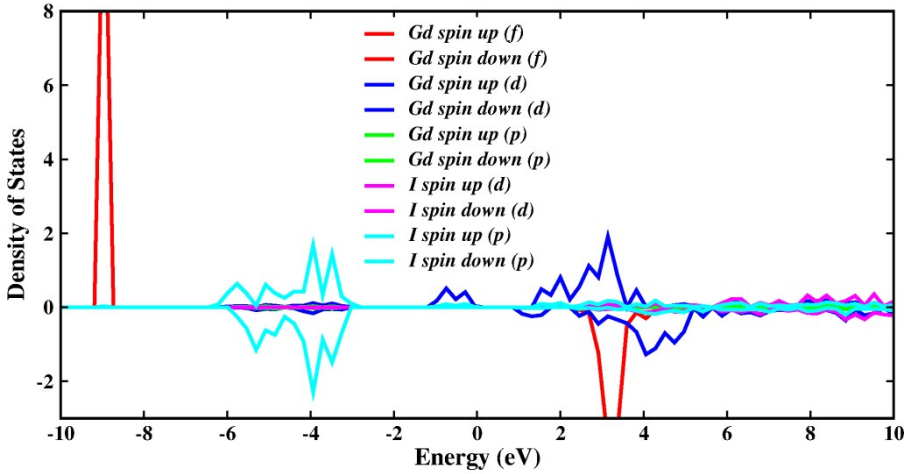

Figure S4. Corresponding orbital-projected densities of states of GdI_2 monolayer.

6. Magnetic Anisotropy Energies for 2D GdI_2 monolayer

Table S1. Summary of Magnetic Anisotropy Energies in μeV/Gd and easy axis (EA) for 2D GdI_2 monolayer.

	d_1	d_2	θ	E(100)-E(001)	E(010)-E(001)	EA
-4% GdI_2	3.96	3.11	79	-556	-556	*xy* plane
GdI_2	4.13	3.14	82	-557	-557	*xy* plane
4% GdI_2	4.29	3.18	85	-769	-769	*xy* plane

7. Relationship between band gaps and Curie temperature T_c in monolayer 2D

ferromagnetic semiconductors.

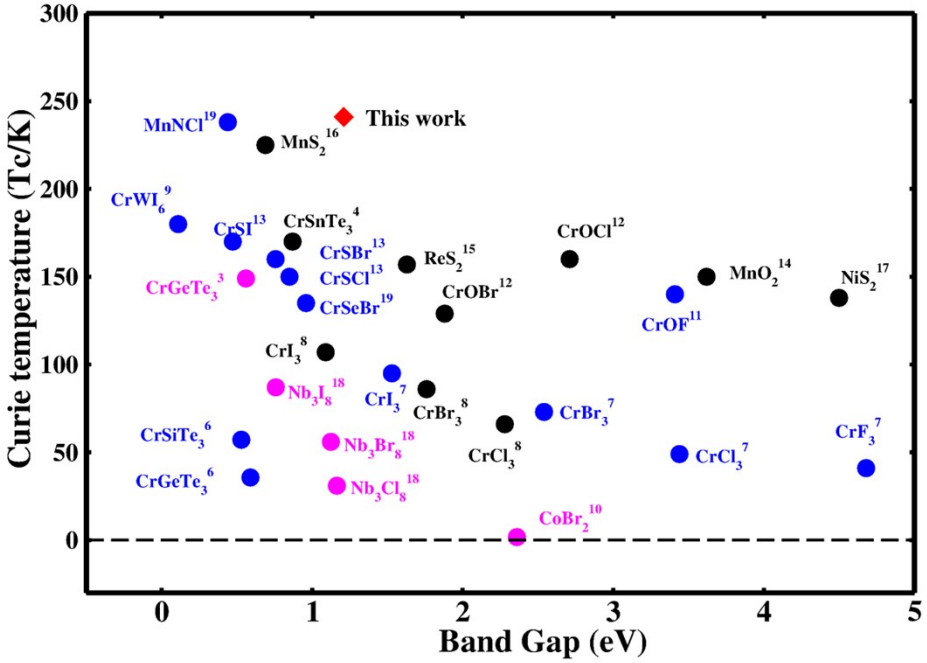

Figure S5. Band gaps and Curie temperature (T_C/K) of 2D FMS monolayers which are possibly exfoliated from their vdW bulk crystals, which are collected with our utmost endeavor from the available published papers. The calculated T_C are estimated based on Heisenberg model (blue), Ising model (black), and mean-field approximation theory (magenta circles), respectively. It can be seen that T_C for GdI_2 monolayer based on Heisenberg model is as high as 241 K, which is significantly higher than those ever reported 2D intrinsic FMS experimentally or theoretically based on the collected data. Note that our T_C based on Ising model for GdI_2 is as high as 745 K (Figure S7).

8. Magnetic moment as functions of temperature for 2D FM $CrCl_3$, $CrBr_3$, and CrI_3.

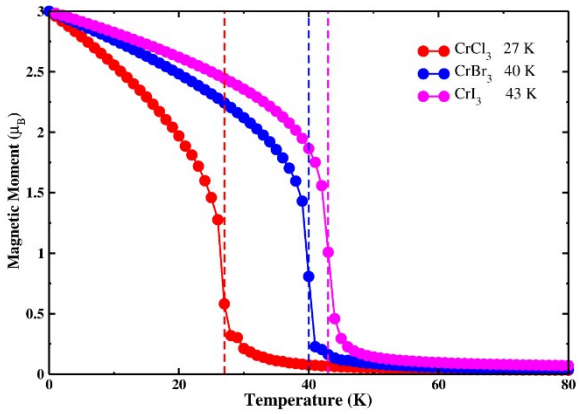

Figure S6. Magnetic moment as functions of temperature for 2D FM $CrCl_3$, $CrBr_3$, and CrI_3, respectively.

To assess the reliability of the method for the prediction of Curie temperature, we also calculated the T_C for the synthesized 2D FM $CrCl_3$, $CrBr_3$, and CrI_3 monolayer based on our Heisenberg model by using Monte Carlo simulations. Using the J values of 5.89, 7.65, and 6.62 meV from our GGA+U (U_{eff} = 3 eV) calculations for $CrCl_3$, $CrBr_3$, and CrI_3, the computed T_C are around 27 K, 40 K, and 43 K (Figure S6), respectively, which are in good agreement with the experimental values of 17 K,[20] 34 K,[21] and 45 K.[22]

9. Magnetic moment, magnetic susceptibility, and specific heat as functions of temperature for GdI_2 monolayer based on Ising model.

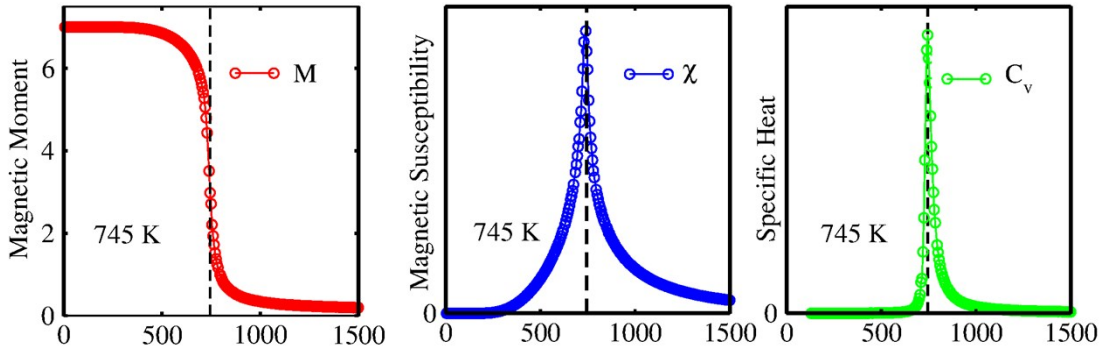

Figure S7. Magnetic moment M (red), magnetic susceptibility χ (blue), and specific heat C_V (green) as functions of temperature for GdI_2 monolayer based on Ising model.

10. Band structure and Curie temperature of GdI_2 monolayer under -4% and 4%.

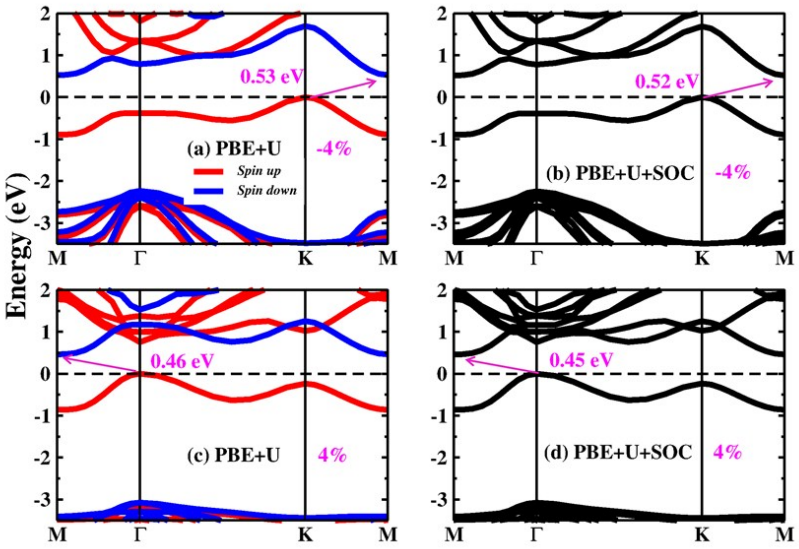

Figure S8. Band structure of -4% and 4% GdI_2 at PBE+U (a, c) and PBE+U+SOC (b, d) level.

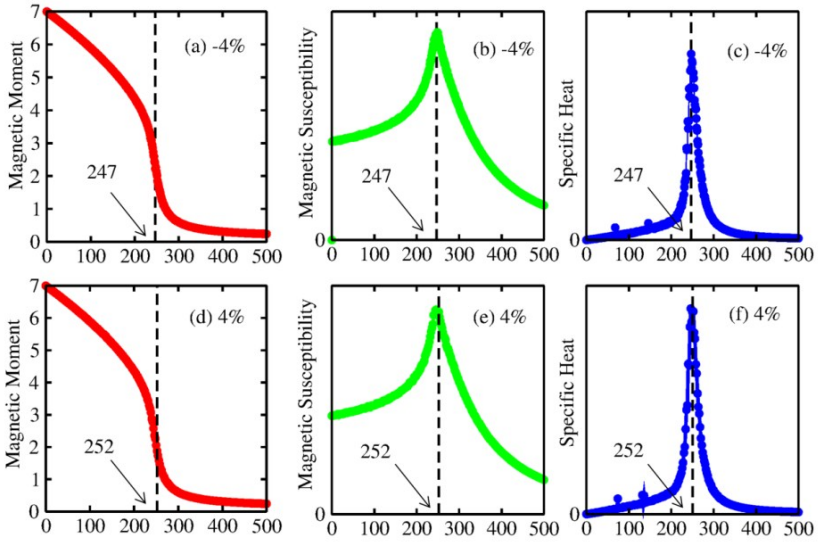

Figure S9. Magnetic moment M (red), specific heat C_V (green), and magnetic susceptibility χ (blue) as functions of temperature for GdI_2 monolayer based on Heisenberg model under -4% and 4% strain, respectively.

11. Stability and relative energy of GdI_2 monolayer under different strains.

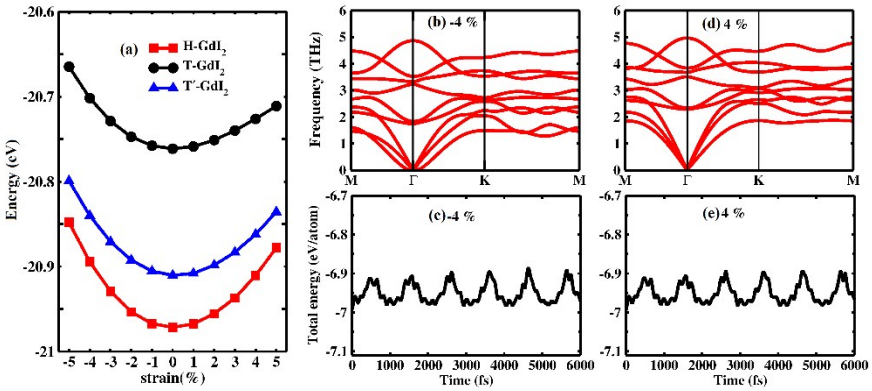

Figure S10. (a) Relative energy of H, T, and T′ GdI_2 monolayer under different strains. The dynamic and thermal stability of GdI_2 monolayer under strain -4% (b, c) and 4% (d, e);

Different phases like T and T′ phases for GdI_2 monolayer were also considered and they possess much higher energy than H-phase under the investigated strain (-5%~5%), therefore, phase transformation should be very hard to happen (Figure S10a). Under strain 4% and 4%, the dynamic and thermal stability of GdI_2 monolayer were confirmed by phonon dispersion calculations and ab initio molecular dynamics simulations, respectively (Figure S10b-e).

12. Band structure and Curie temperature of GdI_2 monolayer under different carrier doping concentration.

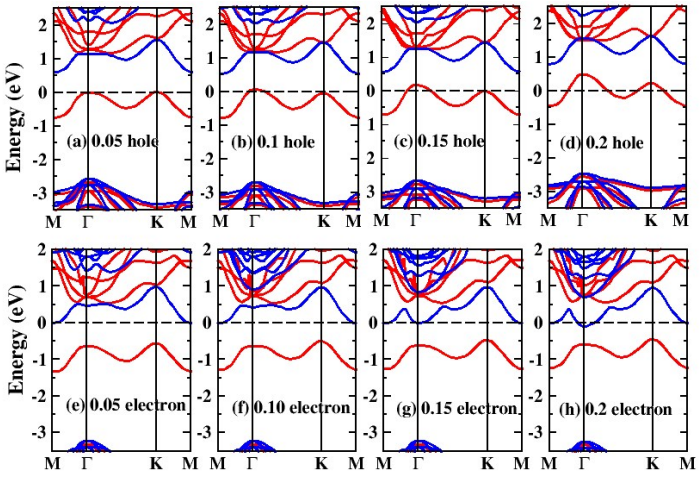

Figure S11. Band structure of hole doping (a-d) and electron doping (e-f) at PBE+U level with the doping concentration of 0.05, 0.1, 0.15, and 0.2 electron or hole per unit cell, respectively.

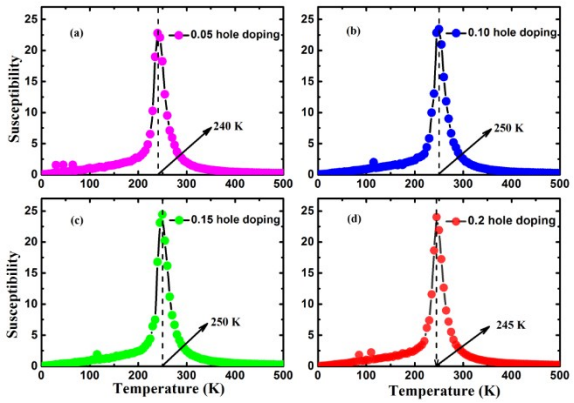

Figure S12. Magnetic susceptibility χ as functions of temperature for GdI_2 monolayer based on Heisenberg model with the doping concentration of 0.05, 0.1, 0.15, and 0.2 hole per unit cell, respectively.

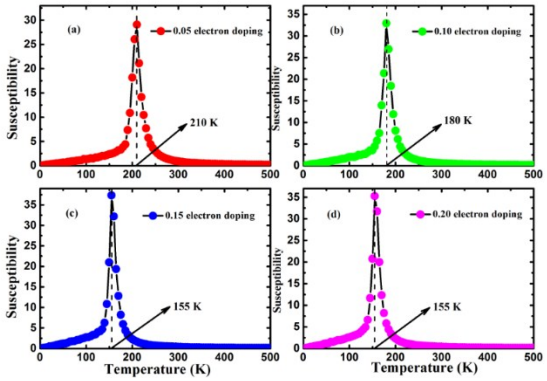

Figure S13. Magnetic susceptibility χ as functions of temperature for GdI_2 monolayer based on Heisenberg model with the doping concentration of 0.05, 0.1, 0.15, and 0.2 electron per unit cell, respectively.

13. Energy difference of GdI_2 monolayer under different U_{eff} values.

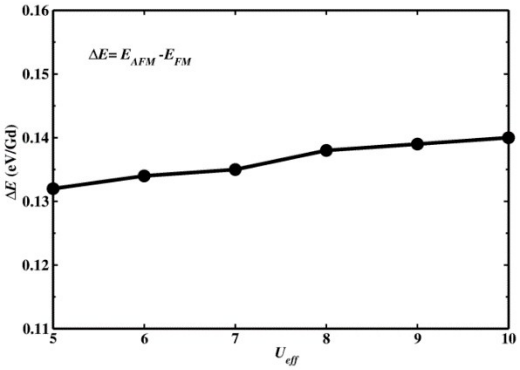

Figure S14. Energy difference of GdI_2 monolayer under different U_{eff} values.

Figure S14 presents the calculated ΔE ($\Delta E = E_{AFM} - E_{FM}$) using GGA+U method with U_{eff} varied from 5 to 10 eV. The result reveals that the FM order of GdI_2

monolayer is the ground state. As can be seen, ΔE increases slightly and saturates to a constant value starting from U_{eff} = 8 eV with the increasing U_{eff}. The magnetic moment (8 μ_B/f.u.) with U_{eff} = 8 eV was also confirmed by using HSE06 hybrid functional (8 μ_B/f.u.). This U_{eff} is also applied on bulk GdI_2, and the calculated lattice constants ($a = b$ = 4.047 Å, c = 14.97 Å) are in good agreement with the experimental values ($a = b$ = 4.075 Å, c = 15.06 Å)[23]. Therefore U_{eff} = 8.0 eV is adopted within the GGA+U calculations.

14. Density of states for single Gd atom at FM and AFM states

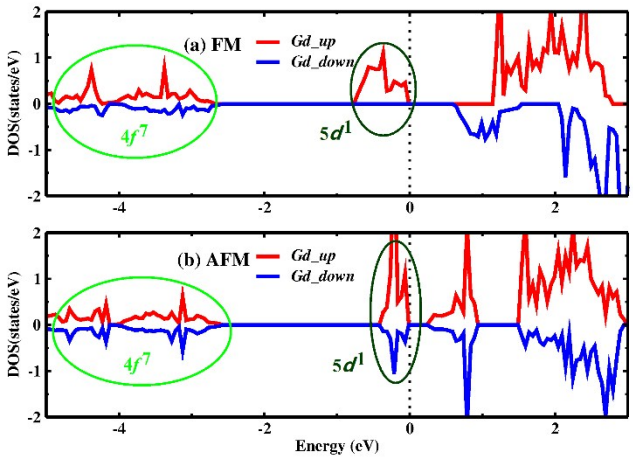

Figure S15. Density of states for single Gd atom at FM and AFM states.

References

1. Andrew, R. C.; Mapasha, R. E.; Ukpong, A. M.; Chetty, N., *Phys. Rev. B* **2012,** *85* (12), 125428.
2. Zhang, H.; Wang, R., *Physica B* **2011,** *406* (21), 4080-4084.
3. Fang, Y.; Wu, S.; Zhu, Z. Z.; Guo, G. Y., *Phys. Rev. B* **2018,** *98* (12), 125416.
4. Zhuang, H. L.; Xie, Y.; Kent, P. R. C.; Ganesh, P., *Phys. Rev. B* **2015,** *92* (3), 035407.
5. Zhou, L.; Kou, L.; Sun, Y.; Felser, C.; Hu, F.; Shan, G.; Smith, S. C.; Yan, B.; Frauenheim, T., *Nano Lett.* **2015,** *15* (12), 7867-7872.
6. Li, X.; Yang, J., *J. Mater. Chem. C* **2014,** *2* (34), 7071.
7. Zhang, W. B.; Qu, Q.; Zhu, P.; Lam, C. H., *J. Mater. Chem. C* **2015,** *3* (48), 12457-12468.
8. Liu, J.; Sun, Q.; Kawazoe, Y.; Jena, P., *Phys. Chem. Chem. Phys.* **2016,** *18* (13), 8777-8784.
9. Huang, C.; Feng, J.; Wu, F.; Ahmed, D.; Huang, B.; Xiang, H.; Deng, K.; Kan, E., *J. Am. Chem. Soc.* **2018**, 140, 11519−11525.
10. Lv, H. Y.; Lu, W. J.; Luo, X.; Zhu, X. B.; Sun, Y. P., *Phys. Rev. B* **2019,** *99* (13),

134416.
11. Xiao, T.; Wang, G.; Liao, Y., *Chem. Phys.* **2018,** *513*, 182-187.
12. Miao, N.; Xu, B.; Zhu, L.; Zhou, J.; Sun, Z., *J. Am. Chem. Soc.* **2018,** *140* (7), 2417-2420.
13. Guo, Y.; Zhang, Y.; Yuan, S.; Wang, B.; Wang, J., *Nanoscale* **2018,** *10* (37), 18036-18042.
14. Kan, M.; Zhou, J.; Sun, Q.; Kawazoe, Y.; Jena, P., *J. Phys. Chem. Lett.* **2013,** *4* (20), 3382-3386.
15. Sun, Z.; Lv, H.; Zhuo, Z.; Jalil, A.; Zhang, W.; Wu, X.; Yang, J., *J. Mater. Chem. C* **2018,** *6* (5), 1248-1254.
16. Kan, M.; Adhikari, S.; Sun, Q., *Phys. Chem. Chem. Phy.* **2014,** *16* (10), 4990.
17. Kulish, V. V.; Huang, W., *J. Mater. Chem. C* **2017,** *5* (34), 8734-8741.
18. Jiang, J.; Liang, Q.; Meng, R.; Yang, Q.; Tan, C.; Sun, X.; Chen, X., *Nanoscale* **2017,** *9* (9), 2992-3001.
19. Wang, C.; Zhou, X.; Zhou, L.; Tong, N. H.; Lu, Z. Y.; Ji, W., *Sci. Bull.* **2019,** *64* (5), 293-300.
20. Cai, X.; Song, T.; Wilson, N. P.; Clark, G.; He, M.; Zhang, X.; Taniguchi, T.; Watanabe, K.; Yao, W.; Xiao, D.; McGuire, M. A.; Cobden, D. H.; Xu, X., *Nano Lett.* **2019**, 19, 3993-3998
21. Zhang, Z.; Shang, J.; Jiang, C.; Rasmita, A.; Gao, W.; Yu, T., *Nano Lett.* **2019,** *19* (5), 3138-3142.
22. Huang, B.; Clark, G.; Navarro-Moratalla, E.; Klein, D. R.; Cheng, R.; Seyler, K. L.; Zhong, D.; Schmidgall, E.; McGuire, M. A.; Cobden, D. H.; Yao, W.; Xiao, D.; Jarillo-Herrero, P.; Xu, X., *Nature* **2017,** *546* (7657), 270-273.
23. A. Kasten, P. H. Moller and M. Schienle, Solid State Commun., 1984, 51, 919-921.